ACS APPLIED MATERIALS & INTERFACES

Research Article

www.acsami.org

ZnO-based Thin Film Transistors Employing Aluminum Titanate Gate Dielectrics Deposited by Spray Pyrolysis at Ambient Air

Dimitrios Afouxenidis,[†] Riccardo Mazzocco,[‡] Georgios Vourlias,[§] Peter J. Livesley,[‡] Anthony Krier,[‡] William I. Milne,[⊥,∥] Oleg Kolosov,[‡] and George Adamopoulos*[,†]

[†]Engineering Department, Lancaster University, Lancaster LA1 4YR, United Kingdom

[‡]Department of Physics, Lancaster University, Lancaster LA1 4YB, United Kingdom

[§]Physics Department, Aristotle University of Thessaloniki, Thessaloniki 54142, Greece

[⊥]Department of Engineering, University of Cambridge, 9 JJ Thomson Avenue, Cambridge CB3 0FA, United Kingdom

[∥]Display Research Laboratory, Department of Information Display, Kyung Hee University, Seoul 130701, South Korea

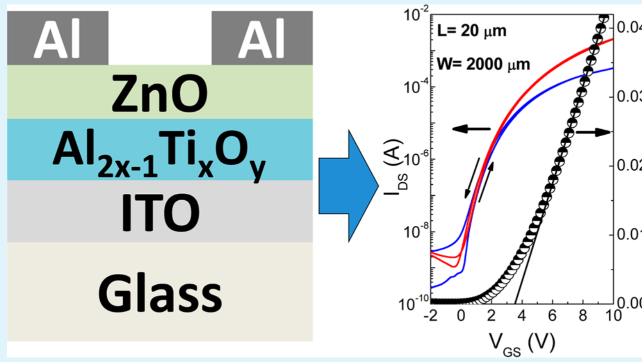

ABSTRACT: The replacement of SiO_2 gate dielectrics with metal oxides of higher dielectric constant has led to the investigation of a wide range of materials with superior properties compared with SiO_2. Despite their attractive properties, these high-*k* dielectrics are usually manufactured using costly vacuum-based techniques. To overcome this bottleneck, research has focused on the development of alternative deposition methods based on solution-processable metal oxides. Here we report the application of spray pyrolysis for the deposition and investigation of $Al_{2x-1}\cdot Ti_xO_y$ dielectrics as a function of the $[Ti^{4+}]/[Ti^{4+}+2\cdot Al^{3+}]$ ratio and their implementation in thin film transistors (TFTs) employing spray-coated ZnO as the active semiconducting channels. The films are studied by UV–visible absorption spectroscopy, spectroscopic ellipsometry, impedance spectroscopy, atomic force microscopy, X-ray diffraction and field-effect measurements. Analyses reveal amorphous $Al_{2x-1}\cdot Ti_xO_y$ dielectrics that exhibit a wide band gap (~4.5 eV), low roughness (~0.9 nm), high dielectric constant ($k \sim 13$), Schottky pinning factor S of ~0.44 and very low leakage currents (<5 nA/cm^2). TFTs employing stoichiometric $Al_2O_3\cdot TiO_2$ gate dielectrics and ZnO semiconducting channels exhibit excellent electron transport characteristics with low operating voltages (~10 V), negligible hysteresis, high on/off current modulation ratio of ~10^6, subthreshold swing (SS) of ~550 mV/dec and electron mobility of ~10 cm^2 V^{-1} s^{-1}.

KEYWORDS: *high-k dielectrics, aluminum titanate, transparent electronics, spray pyrolysis, thin film transistors*

1. INTRODUCTION

Oxide semiconductors-based thin film transistors (TFTs) are a promising technology for application in next-generation thin film transistors, as they offer numerous advantages over competing technologies (organics, amorphous silicon) including high optical transparency, high electron mobilities, excellent chemical stability and processing versatility.[1−5]

Despite their relatively short history, metal oxide semiconductor-based thin film transistors have already been demonstrated with high performance comparable to polycrystalline silicon;[4,6] however, these high-performance metal oxide-based TFTs are usually manufactured using vacuum-based processing methodologies.[4,7]

In spite of their extraordinary performance, vacuum-based deposition techniques still suffer from high manufacturing costs and their limited large area deposition capabilities. To overcome this technology bottleneck, significant research has been focused on the development of alternative deposition processes based on solutions including spin-casting, dip coating and spray pyrolysis.[8,9]

Along with the progress on solution processed metal oxide semiconductors, research toward solution processed gate dielectrics including high-*k* dielectrics, nanodielectrics, electrolyte dielectrics has also been boosted.[8,10−15] However, the vast majority of the reported work employs conventional dielectrics based on SiO_2. Among the high-*k* dielectrics that include a wide range of transition metals[16] and rare earth[17] metal oxides, which can simultaneously enable low leakage currents through the use of thicker films, as well as low-voltage operation, TiO_2[18−21] and Al_2O_3[22−24] are the most characterized compounds. Initially, TiO_2 attracted attention because of its high dielectric permittivity, $k > 50$. However, TiO_2 films exhibit a relatively low band gap (~3.6 eV), high leakage currents, and undesirable crystallization at temperatures of about 400 °C. On the other hand, Al_2O_3 exhibits a very large band gap ($E_g \sim 9$ eV) but has a relatively low $k \sim 9$. Gate dielectric materials with high

Received: January 20, 2015
Accepted: March 16, 2015
Published: March 16, 2015

DOI: 10.1021/acsami.5b00561
ACS Appl. Mater. Interfaces 2015, 7, 7334−7341

dielectric constants are desirable, but the band offset condition that requires a reasonably large band gap should also be satisfied.[25,26] The latter point is of particular concern when wide band gap metal oxide semiconducting channels are being employed as the number of suitable candidate gate dielectric materials to be used will be significantly reduced. The obvious solution to both the low dielectric constant and narrow band gap issues could be the use of an $Al_2O_3{\cdot}TiO_2$ composite dielectric material with combined high permittivity, wide band gap and low leakage current. To that end, $Ti_xAl_{1-x}O_y$ as well as $Al_2O_3{\cdot}TiO_2$ stacked multilayers have been investigated[11,27−29] as candidate gate dielectric materials. Here we study the structural, optical, electronic and dielectric properties of $Al_{2x-1}{\cdot}Ti_xO_y$ gate dielectrics grown by spray pyrolysis at ambient conditions and varying the titanium to aluminum to atomic ratio. Titanium to aluminum to atomic ratio was adjusted by the simple physical blending of the soluble precursors in alcohol-based solutions. We also demonstrate their implementation in high-mobility, low-voltage TFTs based on ZnO semiconducting channels similarly grown by spray pyrolysis.[30] The films' microstructure was investigated using a wide range of characterization techniques including UV−vis absorption spectroscopy, spectroscopic ellipsometry, atomic force microscopy (AFM), X-ray diffraction (XRD) and impedance spectroscopy. Finally, the electron mobility of the spray coated ZnO films was investigated using an optimized bottom-gate, top-contact transistor architecture.

2. EXPERIMENTAL SECTION

2.1. Al_2O_3, TiO_2, $Al_{2x-1}{\cdot}Ti_xO_y$ and ZnO Deposition by Spray Pyrolysis. Aerosols of 50 mg/mL of aluminum chloride ($AlCl_3$), Ti *n*-butoxide ($Ti(OCH_2CH_2CH_2CH_3)_4$) solutions in 2,4-pentanedione and methanol (1:5) were spray coated at 420 °C onto commercially available indium tin oxide (ITO) coated glass (sheet resistivity $R_s \sim 15$ Ohms/□) employing a pneumatic airbrush, held at a vertical distance of about 30 cm. The composites were equally deposited by properly blending $AlCl_3$ and $Ti(OCH_2CH_2CH_2CH_3)_4$ solutions, so that the desired $[Ti^{4+}]$ to $[Ti^{4+}+2{\cdot}Al^{3+}]$ atomic ratio in the solution could be obtained. Aerosols of the precursors and blends were spray-coated for 30 s while the spray coating process was interrupted for 20 s to allow the vapors to settle. The cycle was repeated until films of typical thicknesses in the range between 100 and 200 nm were obtained. Similarly, the ZnO semiconducting channels were spray coated onto the dielectric-coated ITO substrates heated at 400 °C from 25 mg/mL zinc acetate ($(Zn(CH_3CO_2)_2){\cdot}2H_2O$) solutions in methanol until films of typical thickness of ~35 nm were obtained.

2.2. TFTs Fabrication/Characterization. Bottom gate−top contact (BG−TC) transistors were fabricated by employing aluminum (Al) source and drain (S/D) electrodes (60 nm) that were thermally evaporated under high vacuum (10^{-6} mbar) through a shadow mask on the spray coated glass/ITO/composite/ZnO stacks. Device characterization was performed under high vacuum (10^{-6} mbar), at room temperature. Electrical measurements were carried out using an Agilent B1500A semiconductor parameter analyzer. The electron mobility was extracted from the transfer characteristics in both the linear and saturation regime using the gradual channel approximation.

$$\mu_{e,sat} = \frac{L}{C_{oxi}W}\frac{\partial^2 I_D}{\partial V_G{}^2}$$

$$\mu_{e,lin} = \frac{L}{C_{ox}WV_D}\frac{\partial I_D}{\partial V_G}$$

where, C_{ox} is the geometrical capacitance of the dielectric layers and L and W the length and width of the transistor channel, respectively.

The subthreshold slope SS was calculated as the inverse slope of the transfer curve from

$$SS = \frac{\partial V_{GS}}{\partial(\log_{10} I_{DS})}$$

The devices were thermally annealed at 100 °C in air for 30 min prior to their characterization. The latter constitutes a routine process for solution-processed ZnO-based transistors employing aluminum contacts. Although the underlying mechanism is not clear yet, such postannealing in air at 100 °C improved the transistors characteristics by significantly reducing the negative threshold voltage, subthreshold swing and hysteresis. We postulate that devices annealing in air repairs the damaged ZnO lattice by eliminating the uncontrollable oxygen vacancies in the surface of the subjacent ZnO layer.

2.3. Impedance Spectroscopy. Impedance spectroscopy measurements on MIM devices (glass/ITO/dielectric/Al) were performed using a Wayne Kerr 6550B Precision impedance analyzer at frequencies between 100 Hz and 10 MHz applying a 50 mV AC voltage. The Al electrodes were thermally evaporated on the composite under high vacuum (10^{-6} mbar) through a shadow mask.

2.4. Leakage Currents. Voltage−current density characteristics of MIM devices (glass/ITO/dielectric/Al) were performed under vacuum (10^{-6} mbar) using an Agilent B1500A semiconductor parameter analyzer.

2.5. Atomic Force Microscopy. Atomic force microscopy images were taken in contact mode under ambient conditions using a MultiMode scanning probe microscope (MM-SPM) fitted to a Nanoscope IIIa controller unit employing a silicon tip of a radius <10 nm.

2.6. Sheet Resistivity. The sheet resistivity of glass/ITO was measured by applying a four-terminal sensing technique using a Jandel Multi Height Probe system with an Agilent B1500A semiconductor parameter analyzer.

2.7. X-ray Diffraction. Grazing incidence XRD (GIXRD) experiments were performed using a Rigaku Ultima+ diffractometer with Cu Kα radiation operating at 40 kV.

2.8. UV−Vis Absorption Spectroscopy. Optical transmission spectra of dielectrics and composites on fused silica were measured at wavelengths between 190 and 1000 nm using a PerkinElmer Lambda 35 UV−vis spectrophotometer.

2.9. Spectroscopic Ellipsometry. SE measurements of dielectric films on c-Si were performed in ambient conditions at an incidence angle of 70° using a Jobin−Yvon UVISEL phase modulated system at the spectral range between 1.5 and 6 eV.

3. RESULTS AND DISCUSSION

The UV−vis transmission spectra of $Al_{2x-1}{\cdot}Ti_xO_y$ films grown on fused silica substrates with varying $[Ti^{4+}]/[Ti^{4+}+2{\cdot}Al^{3+}]$ atomic ratio were recorded in transmission mode in the range between 190 and 1000 nm. The Tauc plots[31] that show the onset of the optical transitions of the films near the band edge are illustrated in Figure 1. The calculated optical band gap as a function of the $[Ti^{4+}]/[Ti^{4+}+2{\cdot}Al^{3+}]$ ratio is shown in Figure 2.

The optical properties of the $Al_{2x-1}{\cdot}Ti_xO_y$ films on c-Si were investigated independently by ex situ UV−visible spectroscopic ellipsometry within the range of photon energies from 1.5 to 6 eV. The spectra were analyzed in terms of the Lorentz classical model[32] (including the high frequency dielectric constant term ε_∞) using two oscillators that model contributions from low and high energy band-to-band transitions. The derived optical band gaps as a function of the $[Ti^{4+}]/[Ti^{4+}+2{\cdot}Al^{3+}]$ ratio are depicted in Figure 2 and are consistent with the those obtained from the UV−vis absorption spectroscopy.

The optical band gap shows a monotonous decrease with increase in the $[Ti^{4+}]/[Ti^{4+}+2{\cdot}Al^{3+}]$ atomic ratio and varies between the 3.7 eV for anatase TiO_2 and the 6.5 eV for spray-deposited Al_2O_3, respectively. The films were further characterized in terms of the Urbach tail energy (E_u).[33,34] The Urbach tail energy was first associated with electronic

DOI: 10.1021/acsami.5b00561
ACS Appl. Mater. Interfaces 2015, 7, 7334−7341

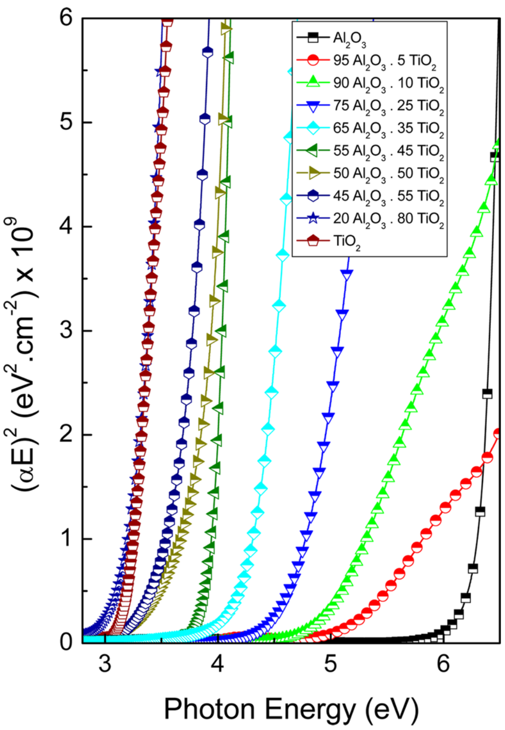

Figure 1. Tauc plots of $Al_{2x-1}\cdot Ti_xO_y$ films as a function of the $[Ti^{4+}]/[Ti^{4+}+2\cdot Al^{3+}]$ atomic ratio.

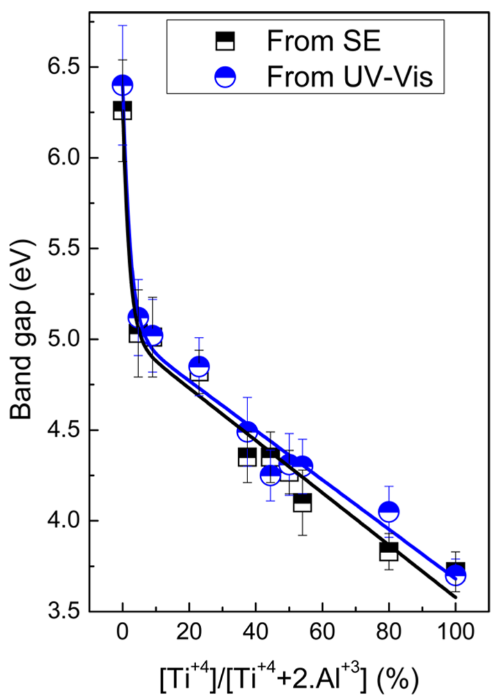

Figure 2. Optical band gap of $Al_{2x-1}\cdot Ti_xO_y$ dielectrics as a function of the $[Ti^{4+}]/[Ti^{4+}+2\cdot Al^{3+}]$ atomic ratio derived from both UV–vis and spectroscopic ellipsometry measurements. The solid lines are a guide to the eye.

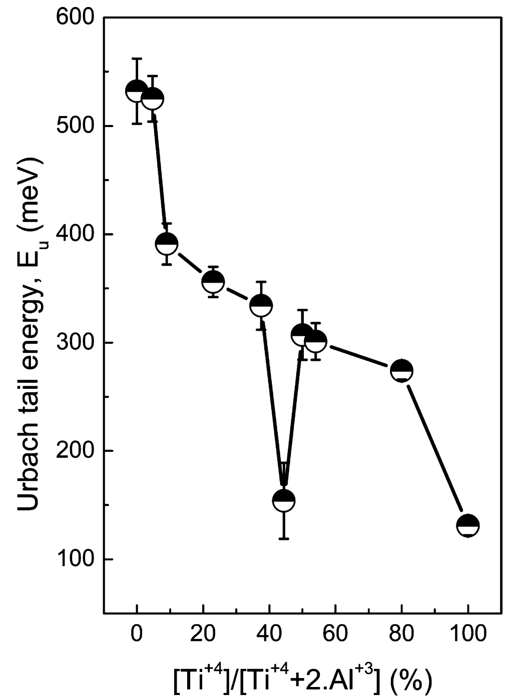

Figure 3. Urbach tail energy (E_u) of $Al_{2x-1}\cdot Ti_xO_y$ dielectrics as a function of $[Ti^{4+}]/[Ti^{4+}+2\cdot Al^{3+}]$ atomic ratio.

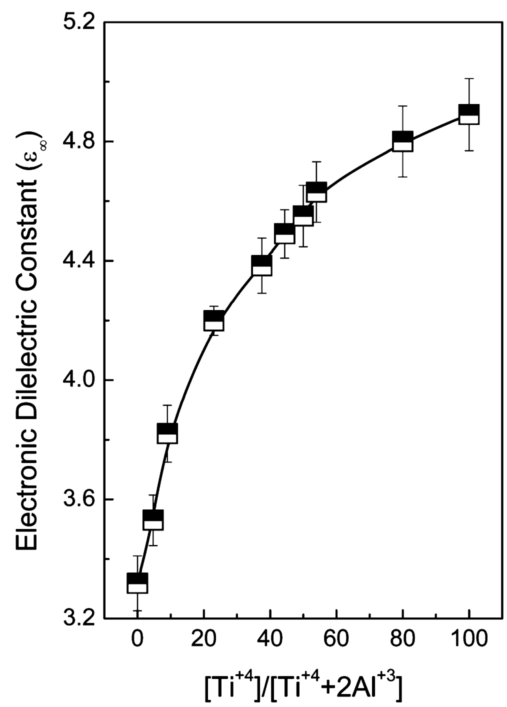

Figure 4. High energy dielectric constant (ε_∞) of $Al_{2x-1}\cdot Ti_xO_y$ dielectrics as a function of $[Ti^{4+}]/[Ti^{4+}+2\cdot Al^{3+}]$ atomic ratio derived from spectroscopic ellipsometry measurements based on Lorentz classical model data modeling. The solid line is a guide to the eye.

transitions from the valence band to the conduction band tail in disordered alkali halides and silver halides. However, during the last few decades, it has been proven to be universal in the study of disorder in numerous systems, differing in structural features, crystal lattice dimensionality, aggregate state, types of phase transitions, low angle grain boundaries, oxygen vacancies, etc.

As shown in Figure 3, the Urbach tail energy of $Al_{2x-1}\cdot Ti_xO_y$ films exhibit a monotonous decrease with increase in the $[Ti^{4+}]/[Ti^{4+}+2\cdot Al^{3+}]$ ratio with a discontinuity at $[Ti^{4+}]/[Ti^{4+}+2\cdot Al^{3+}]$ ~45%, where we postulate stoichiometric $Al_2O_3.TiO_2$ is being grown.

DOI: 10.1021/acsami.5b00561
ACS Appl. Mater. Interfaces 2015, 7, 7334−7341

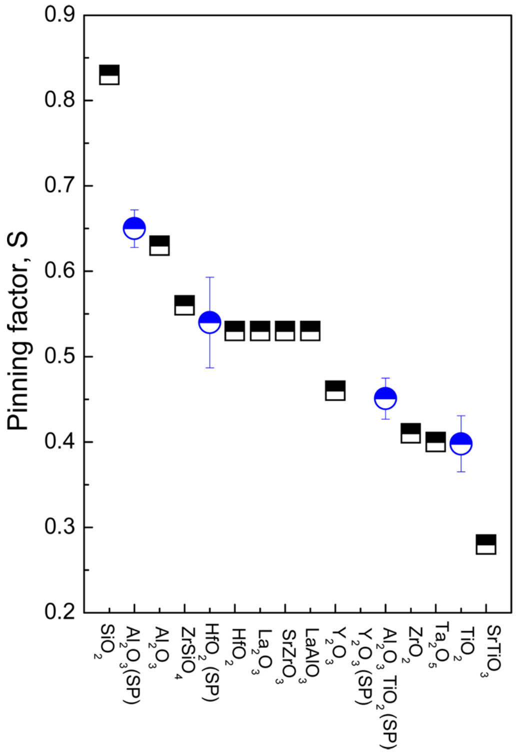

Figure 5. Schottky barrier pinning factor S of solution processed (SP) Al_2O_3, TiO_2, and stoichiometric $Al_2O_3{\cdot}TiO_2$ dielectrics as well as a wide range of dielectrics grown by vacuum-based deposition techniques as well as solutions.

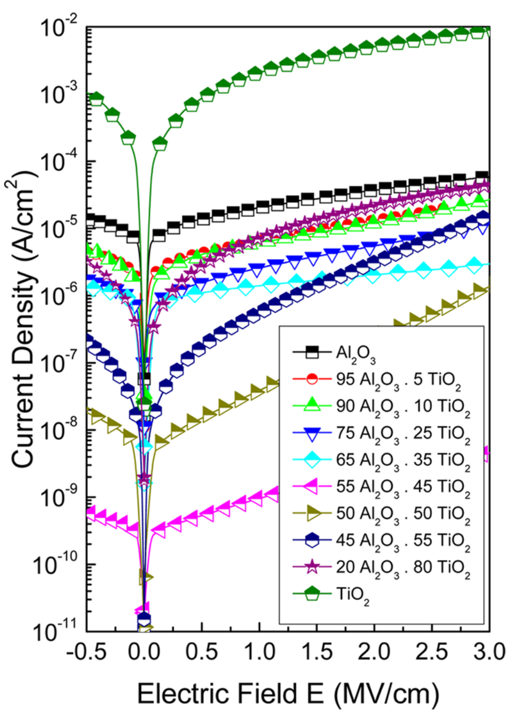

Figure 6. Leakage current density-electric field characteristics of $Al_{2x-1}{\cdot}Ti_xO_y$ solution processed dielectrics as a function of the $[Ti^{4+}]/[Ti^{4+}{+}2{\cdot}Al^{3+}]$ atomic ratio.

The slight divergence around 50% could be explained in terms of the moisture sensitive character of the precursors used in ambient conditions that could potentially result in

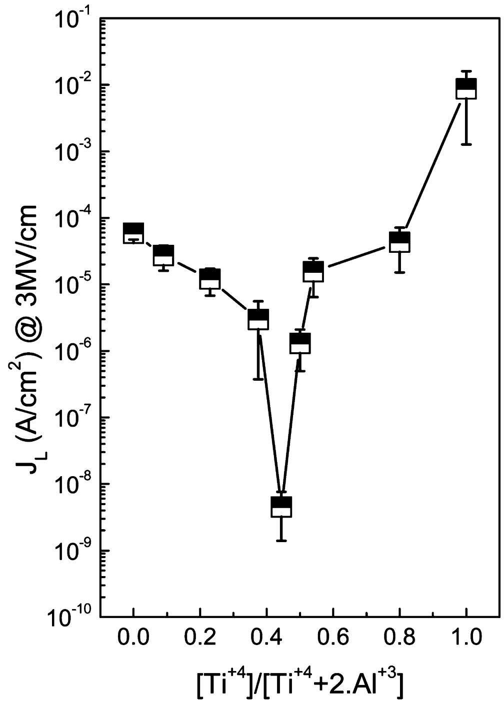

Figure 7. Leakage current density of solution processed $Al_{2x-1}{\cdot}Ti_xO_y$ gate dielectrics at 3 MV cm^{-1} as a function of the $[Ti^{4+}]/[Ti^{4+}{+}2{\cdot}Al^{3+}]$ atomic ratio in the solutions.

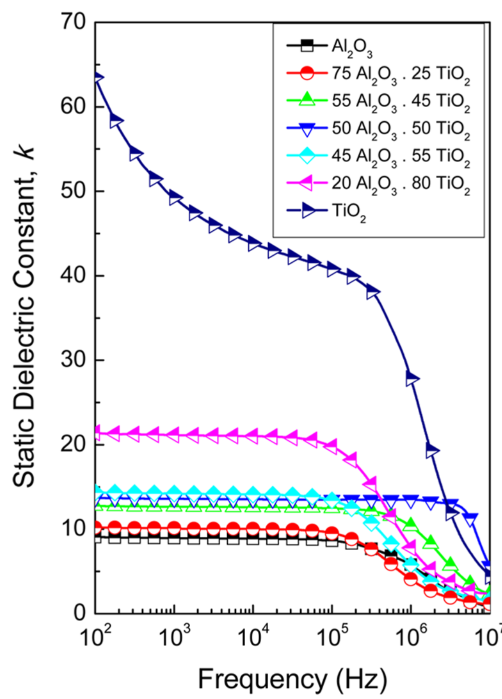

Figure 8. Capacitance dispersions of $Al_{2x-1}{\cdot}Ti_xO_y$ thin films in the frequency range between 100 Hz and 10 MHz.

absorption of H_2O molecules whose mass contribution to the atomic ratio calculations were neglected.

This E_u trend could be interpreted using the formalism of separation of the contributions of static and dynamical structural disordering and can be attributed to a decrease of the dynamic disorder (exciton−phonon coupling) that is expected with the increase in the titanium content and,

DOI: 10.1021/acsami.5b00561
ACS Appl. Mater. Interfaces 2015, 7, 7334−7341

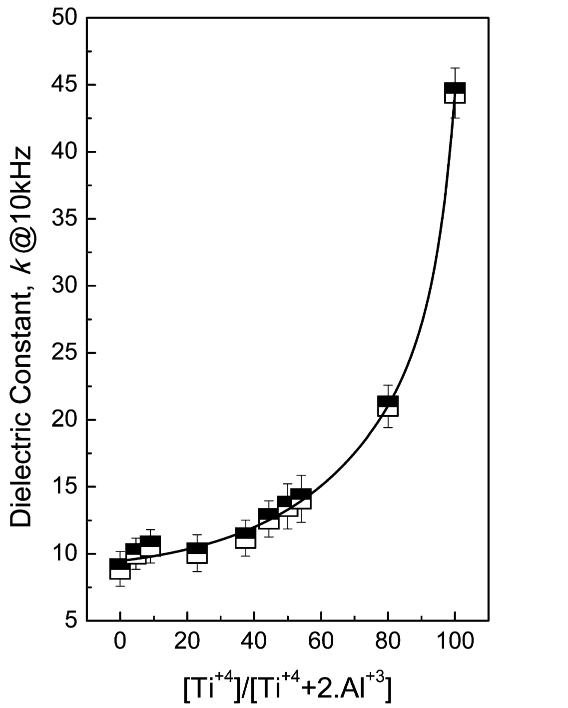

Figure 9. Static dielectric constant of solution processed $Al_{2x-1}\cdot Ti_xO_y$ gate dielectrics versus the $[Ti^{4+}]/[Ti^{4+}+2\cdot Al^{3+}]$ atomic ratio. The solid line is a guide to the eye.

consequently, the inclusion of nanocrystalline TiO_2. However, the sharp decrease of the Urbach tail energy for a $[Ti^{4+}]/[Ti^{4+}+2\cdot Al^{3+}]$ ratio of about 45% (in the solution) in an amorphous (as will be shown later) $Al_{2x-1}\cdot Ti_xO_y$ composite can be attributed to the decrease of the disorder-related parameter of the Urbach tail energy, i.e., decrease of the static disorder in stoichiometric $Al_2O_3\cdot TiO_2$.

The expected monotonous increase of the electronic dielectric constant (ε_∞) obtained from spectroscopic ellipsometry as a function of the $[Ti^{4+}]/[Ti^{4+}+2\cdot Al^{3+}]$ atomic ratio (in the solution) is shown in Figure 4. Based on the electronic dielectric constant (ε_∞), Figure 5 illustrates the Schottky barrier pinning factor, *S*, for Al_2O_3, TiO_2 and solution processed stoichiometric $Al_2O_3\cdot TiO_2$ composite and for comparative purposes a wide range of dielectrics[35] that were deposited from solutions,[12−14] as well as those produced using vacuum deposition techniques.[36−38]

The current−voltage characteristics and dielectric properties of $Al_{2x-1}\cdot Ti_xO_y$ films were assessed by employing a metal−insulator−metal (MIM) device architecture. $Al_{2x-1}\cdot Ti_xO_y$ films of thicknesses in the range between 100 and 200 nm were sandwiched between ITO and Al electrodes. The current-density/electric field characteristics of the stacks are shown in Figure 6. The recorded leakage currents, as a function of the $[Ti^{4+}]/[Ti^{4+}2\cdot Al^{3+}]$ atomic ratio at an electric field of 3 MV/cm, are also depicted in Figure 7. No dielectric breakdown has been observed for electric fields up to 3 MV cm^{-1}. The results demonstrate extremely low leakage currents (<5 nA/cm^2) for $[Ti^{4+}]/[Ti^{4+}+2\cdot Al^{3+}]$ with an atomic ratio of ∼45% where we anticipate stoichiometric $Al_2O_3\cdot TiO_2$ to be produced.

The static dielectric constant dispersions in the range between 100 Hz and 10 MHz are shown in Figure 8. The geometric capacitances that were extracted from the Bode plots at 10 kHz are also illustrated in Figure 9.

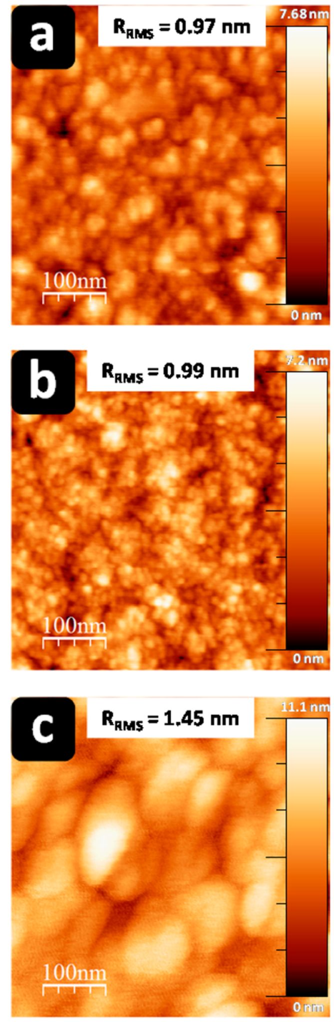

Figure 10. AFM and topography images (RMS roughness inset) of solution processed (a) Al_2O_3, (b) stoichiometric $Al_2O_3\cdot TiO_2$ and (c) TiO_2 dielectrics on glass.

One can immediately observe the monotonous increase of the static dielectric constant with increase in the titanium content and it reaches a value of about 13 for the stoichiometric $[Ti^{4+}]/[Ti^{4+}2\cdot Al^{3+}]$ atomic ratio (in the solution). Also, it should be noted that the dielectric loss of the film deposited from solutions with $[Ti^{4+}]/[Ti^{4+}+2\cdot Al^{3+}]$ ∼ 50% commences at higher frequencies compared to the rest of the $Al_{2x-1}\cdot Ti_xO_y$ composites. The dielectric relaxation at lower frequencies denotes a degradation in the insulating performance of the dielectric thin films, presumably, due to leakage current,[39] as is evidenced in Figure 6. The dielectric relaxation in this study for anatase TiO_2 is a common issue in high-*k* dielectrics;[40] however, a more detailed investigation is outside the scope of this study.

One of the gate dielectric requirements is that the oxide's *k* value should be high enough to be used for a reasonable number of years of scaling; however, there is a tradeoff with the band offset condition,[35] which requires a reasonably large band gap. It is known that the static dielectric constant of candidate oxides tends to vary inversely with the band gap,[26,36−38] so for wide band gap semiconducting channels such as ZnO (E_g = 3.3 eV), a relatively low *k* value could be accepted. Based on our previous findings for the optical band gap, nominal leakage currents and dielectric constant of $Al_{2x-1}\cdot Ti_xO_y$ as a function of

DOI: 10.1021/acsami.5b00561
ACS Appl. Mater. Interfaces 2015, 7, 7334−7341

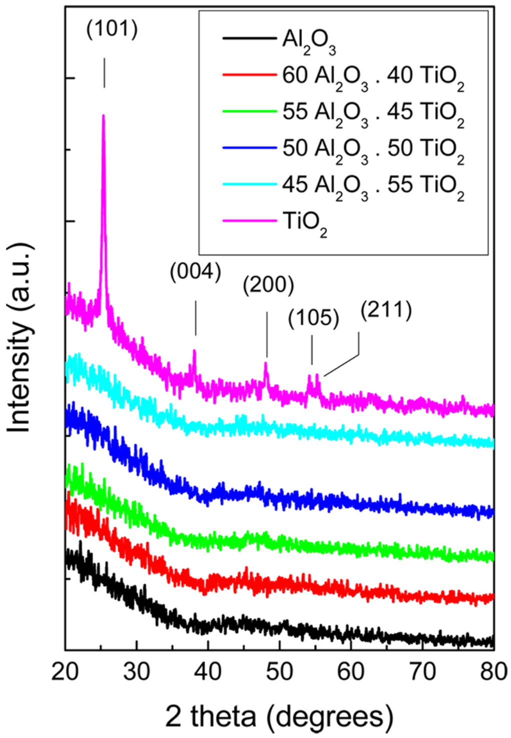

Figure 11. GIXRD patterns of $Al_{2x-1}{\cdot}Ti_xO_y$ dielectrics deposited by SP on glass substrates. Indexing of the patterns (when applicable) is based on tetragonal anatase phase of TiO_2.

the $[Ti^{4+}]/[Ti^{4+}+2{\cdot}Al^{3+}]$ atomic ratio, it appears that stoichiometric $Al_2O_3{\cdot}TiO_2$ should be a promising candidate high-*k* dielectric for ZnO-based thin films transistors.

The surface morphologies of Al_2O_3, $Al_{2x-1}{\cdot}Ti_xO_y$ and TiO_2 films were investigated by atomic force microscopy (AFM). The topography images of the layers that are depicted in Figure 10 demonstrate films of low roughness (~1 nm for stoichiometric $Al_2O_3{\cdot}TiO_2$), a desired characteristic for the implementation of $Al_{2x-1}{\cdot}Ti_xO_y$ dielectrics into thin film transistors. The images presented are the raw images after they have been simply flattened out. Further image processing (e.g., for tip dilation) was omitted, as it had no effect on the image quality. The films' surface roughness was calculated in terms of root-mean-square and found to be ~0.97, ~0.99 and ~1.45 nm for Al_2O_3, stoichiometric $Al_2O_3{\cdot}TiO_2$ and TiO_2, respectively. Such low roughness in particular for stoichiometric $Al_2O_3{\cdot}TiO_2$ indicates the promise for the implementation of $Al_{2x-1}{\cdot}Ti_xO_y$ dielectrics into thin film transistors.

The $Al_{2x-1}{\cdot}Ti_xO_y$ films were further characterized by X-ray diffraction. Grazing incidence (GIXRD) diffraction patterns of Al_2O_3, TiO_2 and selected $Al_{2x-1}{\cdot}Ti_xO_y$ films on glass are illustrated in Figure 11. Basal spacings were obtained using the Bragg equations. The average crystallite size for TiO_2 was determined using the Debye−Scherrer formula based on a shape factor of 0.9.

The background contribution mainly due to the glass substrate was subtracted using the Sonnerveld method.[41] As evidenced from the diffraction patterns, no obvious diffraction peaks (ICDD 41-0258, 84-1641, 42-1468, 73-1199, 75-1863, 21-1272) from Al_2TiO_5, TiO_2 or Al_2O_3 were detected for $Al_{2x-1}{\cdot}Ti_xO_y$ films other than pure TiO_2, indicating the amorphous nature of films. Analysis of the (101) diffraction peak of the pure TiO_2 pattern at ~25.3° using the Debye−Scherrer formula yields an average crystallite size of 22 nm. Note that indexing of the TiO_2 pattern is based on the tetragonal anatase phase (ICDD 21-1272) of TiO_2 (space group $I4_1/amd$) and further pattern analysis provided with the lattice parameters a = 3.7763 Å and c = 9.4471 Å in excellent agreement with previously reported values.[42,43]

The performance of $Al_{2x-1}{\cdot}Ti_xO_y$ films as gate dielectrics was investigated in a bottom-gate, top-contact (BG−TC) TFT architecture (inset, Figures 12 and 13) employing spray coated ZnO as the channel semiconductor. $Al_{2x-1}{\cdot}Ti_xO_y$ composites

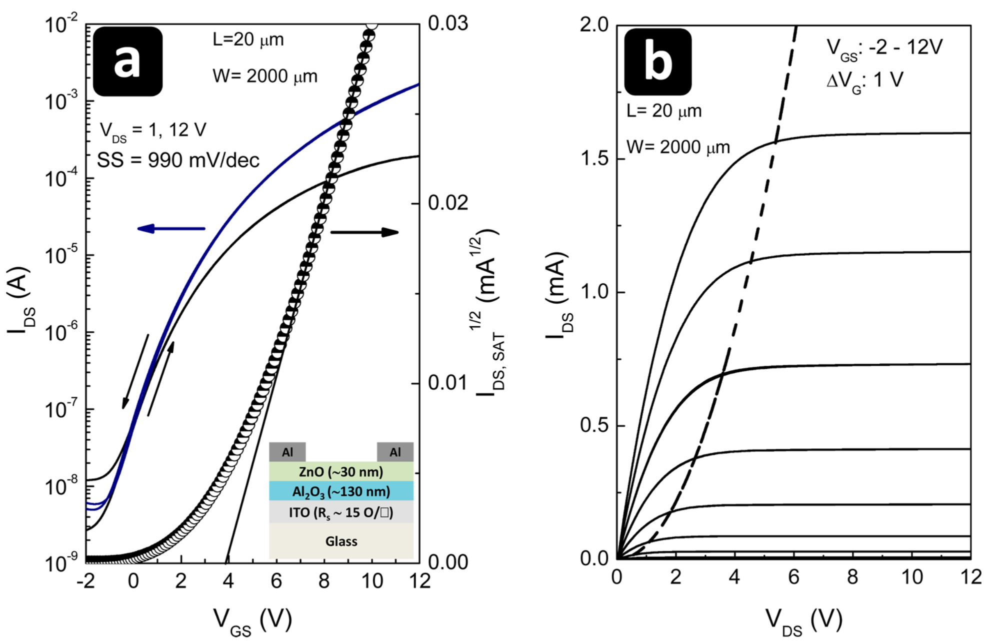

Figure 12. (a) Linear (V_{DS} = 1 V) and saturated (V_{DS} = 12 V) transfer characteristics of bottom-gate, top-contact (inset: architecture employed) TFTs with channel width W = 2000 μm and channel length L = 20 μm, fabricated with spray coated ZnO films on a 60 nF/cm^2 Al_2O_3 dielectric by SP. (b) Output characteristics of ZnO TFT employing SP deposited Al_2O_3 gate dielectric.

DOI: 10.1021/acsami.5b00561
ACS Appl. Mater. Interfaces 2015, 7, 7334−7341

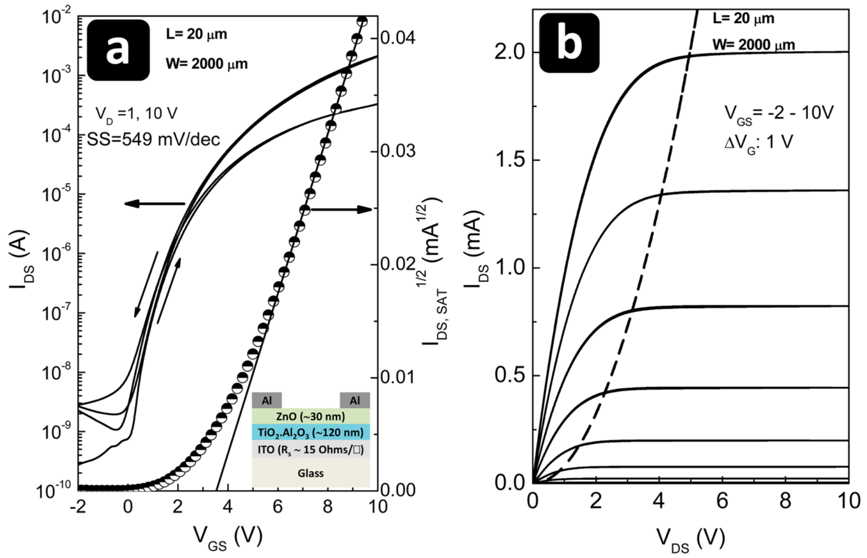

Figure 13. (a) Linear (V_{DS} = 1 V) and saturated (V_{DS} = 10 V) transfer characteristics of bottom-gate, top-contact (inset: architecture employed) TFTs with channel width W = 2000 μm and channel length L = 20 μm, fabricated with spray coated ZnO films on a 90 nF/cm^2 $Al_{2x-1}\cdot Ti_xO_y$ ($[Ti^{4+}]/[Ti^{4+}+2\cdot Al^{3+}]$ ~ 45%) dielectric by SP. (b) Output characteristics of ZnO TFT employing SP deposited $Al_{2x-1}\cdot Ti_xO_y$ ($[Ti^{4+}]/[Ti^{4+}+2\cdot Al^{3+}]$ ~ 45%) gate dielectric.

were deposited by spray pyrolysis (at ~420 °C) onto ITO electrodes followed by the sequential deposition of ZnO (~400 °C) under ambient conditions. Device fabrication was completed with the deposition of Al source and drain (S/D) electrodes by thermal evaporation under high vacuum (10^{-7} mbar). Figures 12 and 13 show a representative set of transfer and output characteristics obtained from a ZnO TFT (L = 20 μm, W = 2000 μm) based on a ~130 nm thick Al_2O_3 and 120 nm thick stoichiometric $Al_2O_3\cdot TiO_2$ ($[Ti^{4+}]/[Ti^{4+}+2\cdot Al^{3+}]$ ~ 45% in the solution) high-k dielectric, respectively. The TFTs exhibit excellent operating characteristics with negligible hysteresis and high current on/off ratio electron mobility of approximately 10 cm^2 V^{-1} s^{-1}. Implementing stoichiometric $Al_2O_3\cdot TiO_2$ rather than Al_2O_3 as a gate dielectric did not affect the electron mobility; however, the current modulation ratio was improved by 1 order of magnitude (10^5 for Al_2O_3 and 10^6 for stoichiometric $Al_2O_3\cdot TiO_2$) and the subthreshold swing (SS) decreased to 441 mV/dec (990 mV dec^{-1} for Al_2O_3 and 549 mV dec^{-1} for stoichiometric $Al_2O_3\cdot TiO_2$). It should be noted that the implementation of TiO_2 as a gate dielectric in ZnO-based TFTs was unsuccessful probably due to negative band offsets between TiO_2 and ZnO.

4. CONCLUSION

We have investigated solution processed large area $Al_{2x-1}\cdot Ti_xO_y$ gate dielectrics under ambient conditions with varying $[Ti^{4+}]/[Ti^{4+}+2\cdot Al^{3+}]$ atomic ratios and also investigated their implementation in spray coated ZnO-based transistors. The physical properties of $Al_{2x-1}\cdot Ti_xO_y$ gate dielectrics were investigated using a wide range of characterization techniques that revealed smooth $Al_{2x-1}\cdot Ti_xO_y$ composites with a wide band gap, high-k, high transparency and an amorphous phase. In particular, stoichiometric $Al_2O_3\cdot TiO_2$ films show very low leakage currents (<5 nA/cm^2 at 3 MV cm^{-1}), high dielectric constant, k ~ 13, wide band gap E_g ~ 4.5 eV and a Schottky pinning factor, S ~ 0.44. The ZnO-based TFTs that were also manufactured from solutions employing stoichiometric $Al_2O_3\cdot TiO_2$ dielectrics showed excellent characteristics, i.e., electron mobilities of ~10 cm^2/(V s), negligible hysteresis, and improved (compared to solution processed Al_2O_3 gate dielectrics) on/off current modulation ratio and subthreshold swing of 10^6 and 549 mV/dec, respectively. In addition, the excellent reproducibility over large areas indicates the potential for the rapid development of transparent oxide electronics at low manufacturing cost employing solution processing paradigms.

■ AUTHOR INFORMATION

Corresponding Author

*Dr. George Adamopoulos. Email: g.adamopoulos@lancaster.ac.uk.

Notes

The authors declare no competing financial interest.

■ ACKNOWLEDGMENTS

The author O.V.K. acknowledges support of EPSRC grant EP/K023373/1 and EU grant FUNPROB.

■ REFERENCES

(1) Nomura, K.; Ohta, H. A.; Takagi, H.; Kamiya, T.; Hirano, M.; Hosono, H. Room-Temperature Fabrication of Transparent Flexible Thin-Film Transistors Using Amorphous Oxide Semiconductors. *Nature* **2004**, *432*, 488–492.

(2) Nomura, K.; Ohta, H.; Ueda, K.; Kamiya, T.; Hirano, M.; Hosono, H. Thin-Film Transistor Fabricated in Single-Crystalline Transparent Oxide Semiconductor. *Science* **2003**, *300*, 1269–1272.

(3) Hoffman, R. L.; Norris, B. H.; Wager, J. F. ZnO-based Transparent Thin-Film Transistors. *Appl. Phys. Lett.* **2003**, *82*, 733–735.

(4) Fortunato, E.; Barquinha, P.; Martins, R. Oxide Semiconductor Thin-Film Transistors: A Review of Recent Advances. *Adv. Mater.* **2012**, *24*, 2945–2986.

(5) Facchetti, A.; Marks, T. *Transparent Electronics: From Synthesis to Applications*; John Wiley & Sons Ltd.: Chichester, U. K., 2010.

(6) Fortunato, E.; Barquinha, P.; Pimentel, A.; Pereira, L.; Goncalves, G.; Martins, R. Amorphous IZO TTFTs with Saturation Mobilities Exceeding 100 cm^2/Vs. *Phys. Status Solidi RRL* **2007**, *1*, R34–6.

DOI: 10.1021/acsami.5b00561
ACS Appl. Mater. Interfaces 2015, 7, 7334–7341

(7) Wang, L.; Yoon, M. H.; Lu, G.; Yang, Y.; Facchetti, A.; Marks, T. J. High-Performance Transparent Inorganic−Organic Hybrid Thin-Film *n*-Type Transistors. *Nat. Mater.* **2006**, *5*, 893−900.

(8) Banger, K. K.; Yamashita, Y.; Mori, K.; Peterson, R. L.; Leedham, T.; Rickard, J.; Sirringhaus, H. Low-Temperature, High-Performance Solution-Processed Metal Oxide Thin-Film Transistors Formed by a "Sol−Gel on Chip" process. *Nat. Mater.* **2010**, *10*, 45−50.

(9) Thomas, S. R.; Pattanasattayavong, P.; Anthopoulos, T. D. Solution-Processable Metal Oxide Semiconductors for Thin-Film Transistor Applications. *Chem. Soc. Rev.* **2013**, *42*, 6910−6923.

(10) Pal, B. N.; Dhar, B. M.; See, K. C.; Katz, H. E. Solution-Deposited Sodium Beta-Alumina Gate Dielectrics for Low-Voltage and Transparent Field-Effect Transistors. *Nat. Mater.* **2009**, *8*, 898−903.

(11) Fortunato, E.; Barros, R.; Barquinha, P.; Figueiredo, V.; Park, S.-H. K.; Hwang, C.-S.; Martins, R. Transparent *p*-Type SnO_x Thin Film Transistors Produced by Reactive rf Magnetron Sputtering Followed by Low Temperature Annealing. *Appl. Phys. Lett.* **2010**, *97*, 052105-1−052105-3.

(12) Esro, M.; Vourlias, G.; Somerton, C.; Milne, W. I.; Adamopoulos, G. High-Mobility ZnO Thin Film Transistors Based on Solution-Processed Hafnium Oxide Gate Dielectrics. *Adv. Funct. Mater.* **2015**, *25*, 134−141.

(13) Adamopoulos, G.; Thomas, S.; Bradley, D. D. C.; McLachlan, M. A.; Anthopoulos, T. D. Low-Voltage ZnO Thin-Film Transistors Based on Y_2O_3 and Al_2O_3 High-k Dielectrics Deposited by Spray Pyrolysis in Air. *Appl. Phys. Lett.* **2011**, *98*, 123503-1−123503-3.

(14) Adamopoulos, G.; Thomas, S.; Wöbkenberg, P. H.; Bradley, D. D. C.; McLachlan, M. A.; Anthopoulos, T. D. High-Mobility Low-Voltage ZnO and Li-Doped ZnO Transistors Based on ZrO_2 High-*k* Dielectric Grown by Spray Pyrolysis in Ambient Air. *Adv. Mater.* **2011**, *23*, 1894−1898.

(15) Liu, J.; Buchholz, B. D.; Chang, R. P. H.; Facchetti, A.; Marks, T. J. High-Performance Flexible Transparent Thin-Film Transistors Using a Hybrid Gate Dielectric and an Amorphous Zinc Indium Tin Oxide Channel. *Adv. Mater.* **2010**, *22*, 2333−2337.

(16) Engel-Herbert, R.; Hwang, Y.; Cagnon, J.; Stemmer, S. Metal-Oxide-Semiconductor Capacitors with ZrO_2 Dielectrics Grown on $In_{0.53}Ga_{0.47}As$ by Chemical Beam Deposition. *Appl. Phys. Lett.* **2009**, *95*, 062908−1−062908−3.

(17) Stemmer, S.; Maria, J. P.; Kingon, A. I. Structure and Stability of La_2O_3/SiO_2 Layers on Si(001). *Appl. Phys. Lett.* **2001**, *79*, 102−104.

(18) Campbell, S. A.; Kim, H. S.; Gilmer, D. C.; He, B.; Ma, T.; Gladfelter, W. L. Titanium Dioxide (TiO_2)-based Gate Insulators. *IBM J. Res. Develop.* **1999**, *43*, 383−392.

(19) Fuyuki, T.; Matsunami, H. Electronic Properties of the Interface between Si and TiO_2 Deposited at Very Low Temperatures. *Jpn. J. Appl. Phys.* **1986**, *25*, 1288−1291.

(20) Rausch, N.; Burte, E. P. Thin TiO_2 Films Prepared by Low Pressure Chemical Vapor Deposition. *J. Electrochem. Soc.* **1993**, *140*, 145−149.

(21) Kim, H. S.; Campbell, S. A.; Gilmer, D. C. Charge Trapping and Degradation in High-Permittivity TiO_2 Dielectric Films. *IEEE Electron Device Lett.* **1997**, *18*, 465−467.

(22) Ishida, M.; Sawada, K.; Yamaguchi, S.; Nakamura, T.; Suzaki, T. Heteroepitaxial $Si/Al_2O_3/Si$ Structures. *Appl. Phys. Lett.* **1989**, *55*, 556−558.

(23) No, S. Y; Eom, D.; Hwang, C. S.; Kim, H. J. Property Changes of Aluminum Oxide Thin Films Deposited by Atomic Layer Deposition under Photon Radiation. *J. Electrochem. Soc.* **2006**, *153*, F87−F93.

(24) Kim, Y.; Lee, S. M.; Park, C. S.; Lee, S. I.; Lee, M. Y. Substrate Dependence on the Optical Properties of Al_2O_3 Films Grown by Atomic Layer Deposition. *Appl. Phys. Lett.* **1997**, *71*, 3604−3606.

(25) Wallace, R. M.; Wilk, G. High-k Gate Dielectric Materials. *MRS Bull.* **2002**, *27*, 192−197.

(26) Robertson, J. Band Offsets of Wide-Band-Gap Oxides and Implications for Future Electronic Devices. *J. Vac. Sci. Technol., B: Microelectron. Nanometer Struct.—Process., Meas., Phenom.* **2000**, *18*, 1785−1791.

(27) Auciello, O.; Fan, W.; Kabius, B.; Saha, S.; Carlisle, J. A.; Chang, R. P. H.; Lopez, C.; Baragiola, R. A. Hybrid Titanium−Aluminum Oxide Layer as Alternative High-*k* Gate Dielectric for the Next Generation of Complementary Metal−Oxide−Semiconductor Devices. *Appl. Phys. Lett.* **2005**, *86*, 042904-1−042904-3.

(28) Shi, L.; Xia, Y. D.; Xu, B.; Yin, J.; Liu, Z. G. Thermal stability and Electrical Properties of Titanium-Aluminum Oxide Ultrathin Films as High-k Gate Dielectric Materials. *J. Appl. Phys.* **2007**, *101*, 034102-1−034102-4.

(29) Fortunato, E.; Figueiredo, V.; Barquinha, P.; Elamurugu, E.; Barros, R.; Goncalves, G.; Park, S. H. K.; Hwang, C. S.; Martins, R. Thin-Film Transistors Based on *p*-Type Cu_2O Thin Films Produced at Room Temperature. *Appl. Phys. Lett.* **2010**, *96*, 192102-1−192102-3.

(30) Adamopoulos, G.; Bashir, A.; Gillin, W. P.; Georgakopoulos, S.; Shkunov, M.; Baklar, M. A.; Stingelin, N.; Bradley, D. D. C.; Anthopoulos, T. D. Structural and Electrical Characterization of ZnO Films Grown by Spray Pyrolysis and Their Application in Thin-Film Transistors. *Adv. Funct. Mater.* **2011**, *21*, 525−531.

(31) Tauc, J. *Optical Properties of Solids*; Abeles, F., Ed.; North-Holland: Amsterdam, 1971.

(32) Wooten, F. *Optical Properties of Solids*; Academic Press: New York, 1972.

(33) Urbach, F. The Long-Wavelength Edge of Photographic Sensitivity and of the Electronic Absorption of Solids. *Phys. Rev.* **1953**, *92*, 1324−1324.

(34) Dunstan, D. J. Evidence for a Common Origin of the Urbach Tails in Amorphous and Crystalline Semiconductors. *J. Phys. C: Solid State Phys.* **1982**, *30*, L419−L424.

(35) Mönch, W. Metal-Semiconductor Contacts: Electronic Properties. *Surf. Sci.* **1994**, *300*, 928−944.

(36) Kittl, J. A.; Opsomer, K.; Popovici, M.; Menou, N.; Kaczer, B.; Wang, X. P.; Adelmann, C.; Pawlak, M. A.; Tomida, K.; Rothschild, A.; Govoreanu, B.; Degraev, R.; Schaekers, M.; Zahid, M.; Delabie, A.; Meersschaut, J.; Polspoel, W.; Clima, S.; Pourtois, G.; Knaepen, W.; Detavernier, C.; Afanas'ev, V. V.; Blomberg, T.; Pierreux, D.; Swert, J.; Fischer, P.; Maes, J. W.; Manger, D.; Vandervorst, W.; Conard, T.; Franquet, A.; Favia, P.; Bende, H.; Brij, B.; Van Elshocht, S.; Jurczak, M.; Van Houdt, J.; Wouters, D. J. High-k Dielectrics for Future Generation Memory Devices. *Microelectron. Eng.* **2009**, *86*, 1789−1765.

(37) Robertson, J. High k Dielectrics for Future CMOS Devices. *ECS Trans.* **2009**, *19*, 579−591.

(38) Robertson, J. High Dielectric Constant Gate Oxides for Metal Oxide Si Transistors. *Rep. Prog. Phys.* **2006**, *69*, 327−396.

(39) Tang, H.; Prasad, K.; Sanjines, R.; Schmidt, P. E.; Levy, F. Electrical and Optical Properties of TiO_2 Anatase Thin Films. *J. Appl. Phys.* **1994**, *75*, 2042−2047.

(40) Zhao, C.; Zhao, C. Z.; Werner, M.; Taylor, S.; Chalker, P. Dielectric Relaxation of High-*k* Oxides. *Nanoscale Res. Lett.* **2013**, *8*, 456.

(41) Sonneveld, E. J.; Visser, J. W. Automatic Collection of Powder Data from Photographs. *J. Appl. Crystallogr.* **1975**, *8*, 1−7.

(42) Peters, G.; Vill, V. *Index of Modern Inorganic Compounds. Subvolume A. Landolt-Bornstein Numerical Data and Functional Relationships in Science and Technology* Springer Verlag: Berlin, 1989.

(43) Hanaor, D. A. H.; Sorrell, C. C. Review of the Anatase to Rutile Phase Transformation. *J. Mater. Sci.* **2011**, *46*, 855−874.

DOI: 10.1021/acsami.5b00561
ACS Appl. Mater. Interfaces 2015, 7, 7334−7341